Wave Direction Estimation from Optical Satellite Imagery Using Multi-Stage Gabor Filter

Waranrach Viriyavit Faculty of Informatics Burapha University Chonburi, Thailand waranrach.vi@go.buu.ac.th

Komate Amphawan Faculty of Informatics Burapha University Chonburi, Thailand komate@gmail.com

Chanyut Lisawat Faculty of Informatics Burapha University Chonburi, Thailand 66160295@go.buu.ac.th

Kittipisut Chansri Faculty of Informatics Burapha University Chonburi, Thailand 66160292@go.buu.ac.th

Somrudee Deepaisarn Sirindhorn International Thammasat University Pathum Thani, Thailand somrudee@siit.tu.ac.th

Paweena Kanokhong Sirindhorn International Institute of Technology (SIIT), Institute of Technology (SIIT) Thammasat University Pathum Thani, Thailand 6422800126@g.siit.tu.ac.th

Chakapat Chokchaisiri Sirindhorn International Thammasat University Pathum Thani, Thailand m6622040308@g.siit.tu.ac.th

Woramet Simrum Sirindhorn International Thammasat University Pathum Thani, Thailand 6422771400@g.siit.tu.ac.th

Akkharawoot Takhom Faculty of Engineering Thammasat University Pathum Thani, Thailand takkhara@tu.ac.th

Phutphalla Kong Cambodia Academy of Digital Technology Phnom Penh, Cambodia phutphalla.kong@cadt.edu.kh

Didin Agustian Permadi Institut Teknologi National Bandung Universiti Teknologi Malaysia Bandung, Indonesia didin@itenas.ac.id

Sharifah Hafizah Syed Ariffin Johor Bahru, Malaysia shafizah@utm.my

Surasak Boonkla NECTEC, National Science and

Technology Development Agency Pathum Thani, Thailand surasak.boonkla@nectec.or.th

Kasorn Galajit NECTEC, National Science and Technology Development Agency Pathum Thani, Thailand kasorn.galajit@nectec.or.th

Jessada Karnjana NECTEC, National Science and Technology Development Agency Pathum Thani, Thailand jessada.karnjana@nectec.or.th

Abstract—The direction of incoming waves is a primary force driving coastal erosion, dictating the sediment transport patterns that shape shorelines. Accurate estimation of this parameter is therefore essential for effective coastal management. This paper proposes a robust method for estimating wave direction from high-resolution satellite image patches. The approach utilizes texture analysis based on Gabor filters to identify dominant wave crest orientations, with preprocessing enhanced by contrast limited adaptive histogram equalization (CLAHE). We evaluate three orientation strategies: a baseline standard detection, a high-precision two-stage refinement, and an interpolation-based refinement. The methodology is first validated on a synthetic benchmark image with a known ground truth to establish baseline performance, and then applied to real-world coastal imagery from Thailand. Experiments show that refinement strategies, particularly the two-stage method, significantly improve accuracy in ideal conditions and deliver stable, interpretable estimates on real-world data. On the synthetic benchmark, the twostage refinement achieved a low mean absolute error (MAE) of 0.234°, while on real-world coastal imagery, the interpolation refinement demonstrated strong performance with an MAE of 12.95°. Ultimately, this method provides a scalable, non-intrusive tool for analyzing nearshore wave behavior, while emphasizing that optimal results depend on consistent preprocessing and parameter tuning.

Index Terms—coastal erosion, wave direction estimation, satellite imagery, Gabor filters, texture analysis

I. Introduction

Coastal erosion refers to the process by which shorelines are gradually eroded due to natural forces such as waves, currents, tides, and wind, as well as human-induced activities, such as coastal development and sand mining [1], [2]. In Thailand, this phenomenon has become increasingly significant, particularly along low-lying, sediment-rich coasts such as those of the Gulf of Thailand and the Andaman Sea [3], [4]. A recent 35-year analysis has further highlighted the critical rates of shoreline change in the upper Gulf of Thailand, underscoring the urgent need for advanced monitoring techniques [5].

The impacts of coastal erosion extend beyond physical land loss, affecting both local economies and communities. Coastal infrastructure, tourism, and agriculture suffer damage, while the displacement of residents and the degradation of natural ecosystems worsen their socio-economic vulnerability [6]. For instance, in areas like Bangsaen Beach and Songkhla Lake,

erosion has led to the loss of recreational spaces and reduced safety due to dangerous rip currents [2], [7].

To mitigate these effects, various protection strategies have been implemented, including hard structures such as seawalls, breakwaters, and groins, as well as soft measures like beach nourishment and mangrove planting [6], [8]. These protective structures aim to reduce wave energy and sediment transport, thus stabilizing the shoreline [4], [8].

However, while these interventions can temporarily slow erosion, they are not always successful in the long term and can sometimes cause unintended negative consequences. For example, installing breakwaters can shift erosion to adjacent, unprotected areas or interfere with natural sediment flows [2], [6]. Even after such structures are built, studies still report ongoing shoreline retreat in various locations [7].

This reveals the need for more adaptive and informed coastal management strategies. To improve the effectiveness of protection and prevention measures, it is essential to study the underlying causes of coastal erosion, particularly the dynamic interactions between physical and environmental forces [2], [3]. Key factors include wave direction and height, wind, tides, sediment supply, and coastal currents [1], [2].

Wave direction, in particular, plays a critical role in determining sediment transport patterns and beach morphology [1], [9]. However, although several Thai studies use satellite images to analyze coastal changes and morphology. There is a noticeable gap in the literature when it comes to directly estimating wave direction from satellite imagery [3], [4], [6]. Current approaches primarily use satellite data to observe historical shoreline shifts rather than infer real-time hydrodynamic parameters like wave direction.

Therefore, to enhance the ability to predict and manage coastal erosion in Thailand, there is a compelling need to explore methods that can estimate wave direction directly from satellite images. Such approaches would enable more efficient and large-scale monitoring of coastal dynamics and support the development of better-informed protective strategies.

Traditional in-situ instruments for wave measurement, such as moored buoys and acoustic doppler current profilers (AD-CPs), are prohibitively expensive and provide only sparse, point-based data. Consequently, they fail to capture the critical spatial dynamics of nearshore wave fields, leaving large coastal areas unmonitored [10]–[12].

Therefore, this paper proposes a novel approach to estimate wave direction directly from satellite imagery, addressing the current gap in Thai coastal erosion studies. This study aims to enhance the understanding of wave-induced sediment transport mechanisms. The proposed solution adapts the local gradients method introduced by Koch, Originally designed for wind direction retrieval from synthetic aperture radar (SAR) imagery [13]. This technique calculates local image gradients and derives wind-aligned features based on the most frequent gradient orientations. By modifying and optimizing this algorithm, we aim to estimate the wave direction instead of the wind direction, using high-resolution satellite imagery. Our approach is also adapted from studies that utilize optical

imagery for wave parameter estimation [14], providing a complementary perspective to SAR-based methods [15], [16].

The challenge of coastal erosion is not unique to Thailand; it is a pressing issue for many maritime nations in the ASEAN region that share similar coastal characteristics. Recognizing this shared challenge and the potential for developing transferable monitoring techniques, this research was initiated as part of a collaborative project among several ASEAN member states and Japan, under the ASEAN IVO framework.

II. DATASETS PREPARATION

To establish a baseline and validate the intrinsic accuracy of our proposed methods under ideal conditions, a synthetic benchmark image, named "synthetic grid benchmark," was programmatically generated. The image has dimensions of 1952×1952 pixels and is composed of an 8×8 grid of cells, each 244×244 pixels. Each cell contains a clear, noise-free pattern of parallel lines simulating ideal wave crests with a precisely known orientation. This synthetic dataset provides an absolute ground truth, allowing for a rigorous evaluation of each method's performance without confounding factors from environmental noise or image artifacts, as shown in Fig. 1.

For real-world application, high-resolution satellite images of the coastal region along Chaloem Burapha Chonlathit road (Bang Kachai, Laem Sing, Chanthaburi) were captured using Google Earth Pro. Each image was taken from a top-down perspective aligned to true north, with an eye altitude varying between 600 meters and 1000 meters to balance detail and coverage. Images were exported at 8K resolution to maintain visual clarity.

To facilitate localized analysis, the real-world satellite image was divided into non-overlapping 244×244 pixel patches, resulting in a total of 403 patches for analysis. This process allowed for focused inspection of real-world wave patterns.

Ground truth was established for both datasets. For the "synthetic grid benchmark" image, the ground truth direction for each grid cell is known by design. An example of the ground truth values is illustrated in Fig. 2.

For the real-world patches, where in-situ measurements were unavailable, a reference ground truth was established through manual annotation in GIMP. A line was drawn perpendicular to the dominant, visually identifiable wave crests in each patch, and the resulting angle relative to the vertical axis was recorded. While acknowledging the potential for subjective interpretation, this approach provides a necessary baseline for evaluating the algorithm's performance. To ensure consistency, a single annotator performed all labeling following a standardized protocol. A few ground truth examples are shown in Fig. 3.



Fig. 1. Example portion (i.e., 4×8 grids) of the full 8×8 synthetic grid benchmark image used for validation.

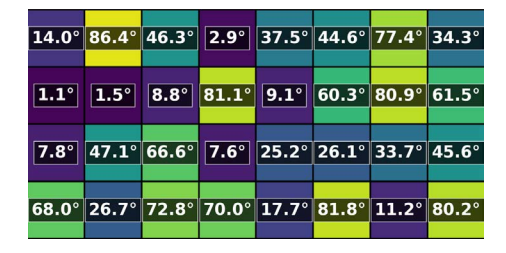


Fig. 2. Visualization of the ground truth angles for an example portion of the synthetic grid benchmark. Each color-coded cell represents the exact, predefined orientation for the corresponding area shown in Fig. 1.

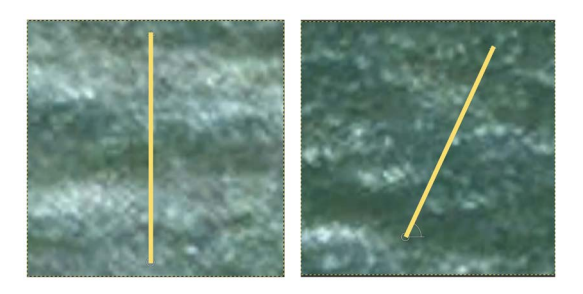


Fig. 3. Examples of the manual ground truth annotation on real-world imagery. The line represents the reference wave direction, drawn perpendicular to the visually dominant wave crests.

III. PROPOSED METHOD

To estimate wave direction from the prepared image patches, we propose a robust methodology based on texture analysis using Gabor filters. This approach is designed to identify the dominant orientation of periodic patterns, such as wave crests, within each patch. The workflow includes patch-level preprocessing, multi-stage orientation analysis, and a dynamic confidence check to ensure the reliability of the estimates, as detailed in the following subsections.

A. Patch Preprocessing

Each image patch undergoes a two-step preprocessing sequence to enhance the visibility of wave patterns for subsequent analysis.

The input color patch is first converted to a single-channel grayscale image. This step simplifies the analysis by focusing on luminance variations, which correspond to the alternating crests and troughs of the wave field.

Second, to accentuate subtle wave features that may be obscured by poor lighting or low contrast, contrast limited

adaptive histogram equalization (CLAHE) is applied. Unlike global equalization, CLAHE operates on local regions (e.g., 8×8 pixel tiles), preventing the over-amplification of noise while effectively sharpening the definition of wave crests. The utility of CLAHE for enhancing features in maritime optical satellite imagery has been validated in recent studies for applications such as ship detection [17].

B. Gabor Filter Bank Generation

The use of Gabor filters for texture analysis is well-established in remote sensing applications, such as sea-ice classification and hyperspectral image analysis [18], [19]. The core of our orientation analysis is a bank of Gabor filters. Gabor filters are widely recognized for their effectiveness in texture analysis and feature extraction due to their ability to capture frequency and orientation information locally [19], [20]. The mathematical form of a 2D Gabor filter in the spatial domain is given by the following equations.

$$g(x, y; \lambda, \theta, \psi, \sigma, \gamma) = \exp(\alpha) \times \cos(\beta),$$
 (1)

$$\alpha = -\frac{x'^2 + \gamma^2 y'^2}{2\sigma^2},\tag{2}$$

and

$$\beta = 2\pi \frac{x'}{\lambda} + \psi,\tag{3}$$

where $x' = x \cos \theta + y \sin \theta$ and $y' = -x \sin \theta + y \cos \theta$, λ is the parameter of the wavelength, θ is orientation, ψ is phase offset, σ is standard deviation of the Gaussian envelope, and γ is spatial aspect ratio.

A filter bank containing 32 Gabor kernels is generated, with each kernel tuned to a specific orientation θ_k for $k \in \{1,...,32\}$, spaced linearly between 0° and 180°. The filter parameters are selected based on empirical observation and established practices. The wavelength (λ) is set to 15 pixels to match the approximate spatial frequency of the observed wave crests. The spatial aspect ratio (γ) is set to 0.6, creating an elliptical filter shape effective for detecting elongated wave lines. This choice is supported by some systematic studies, by Bianconi and Fernández [21], which found that lower γ values (near 0.5) improve classification performance. The phase offset (ψ) is set to 0 to generate an even-symmetric filter optimal for detecting wave ridges. The standard deviation (σ) is set proportionally to λ , a choice consistent with the optimal ratio $(\sigma/\lambda \approx 0.56)$ for effective feature detection [20].

C. Wave Crest Orientation Estimation

For each preprocessed patch I(x,y) at a pixel coordinate (x,y), a response map is generated by convolving the patch with each Gabor kernel g_k from the filter bank. The dominant orientation is found by identifying the filter that produces the maximum mean response magnitude, \bar{M}_k , calculated over all N valid pixels in the patch.

$$\bar{M}_k = \frac{1}{N} \sum_{x,y} |I(x,y) * g_k(x,y)|,$$
 (4)

where * denotes the 2D convolution operation, and N is the total number of pixels of the image patch.

The optimal orientation is given by $\theta_{\rm crest}=\theta_{\hat k}$, The index $\hat k$ is found by maximizing the mean response magnitude, i.e., $\hat k=\arg\max_k \bar M_k$. To improve precision, one of the following three refinements is used.

- 1) Standard Detection: This baseline approach serves as the simplest and most computationally efficient method. It identifies the single Gabor filter from the bank of 32 that elicits the maximum mean energy response (\bar{M}_k) . The orientation of this specific filter is then directly assigned as the wave crest orientation for the patch. The primary limitation of this method is its precision, which is inherently capped by the angular resolution of the filter bank, i.e., 180° / 32 filters = 5.625° . It is best suited for applications requiring a rapid, coarse assessment of the wave field where high angular precision is not the main objective.
- 2) Two-Stage Refinement: This method employs a hierarchical coarse-to-fine search strategy to balance precision with computational cost. In the first stage, the standard detection method is used to identify a coarse, approximate orientation. In the second stage, the analysis zooms in on this angle by generating a new, high-resolution bank of 32 Gabor filters focused only within a narrow angular window, i.e., $\pm 5.625^{\circ}$, around the coarse direction. The final orientation is determined from the peak response in this second, fine-grained search. This approach significantly increases angular precision by concentrating computational effort where it is most needed.
- 3) Interpolation-based Refinement: This technique offers a highly efficient path to sub-resolution precision by using mathematical estimation. It operates on the assumption that the true orientation peak lies between the discrete angles of the initial filter bank. After the standard method identifies the filter with the peak response $(\bar{M}_{\hat{k}})$ and its two immediate neighbors $(\bar{M}_{\hat{k}-1})$ and $\bar{M}_{\hat{k}+1}$, a quadratic polynomial equation is fitted to these three points. The analytical maximum of this polynomial equation is calculated using the following equation, yielding a more precise orientation estimate. This technique, known as parabolic interpolation, allows for sub-resolution accuracy by estimating the true peak of the response function between the discrete angular steps of the filter bank.

$$\delta = \frac{1}{2} \frac{\bar{M}_{\hat{k}-1} - \bar{M}_{\hat{k}+1}}{\bar{M}_{\hat{k}-1} - 2\bar{M}_{\hat{k}} + \bar{M}_{\hat{k}+1}},\tag{5}$$

where δ is the correction factor, which estimates the offset from the sidcrete angle of the winning filter to the true peak of the response curve, and \hat{k} is the index of the Gabor filter that produced the maximum mea response from the initial bank.

The refined crest orientation is then calculated based on the adjusted index $\hat{k} + \delta$. This method achieves precision comparable to the two-stage approach with minimal additional computational overhead.

D. Dynamic Confidence Thresholding

To filter out unreliable estimates from noisy or featureless patches, a dynamic confidence threshold T is employed. This

threshold is calculated based on the global maximum response across the entire source image, ensuring it adapts to varying image conditions.

$$T = f \times \max_{x,y,k} |I_{\text{full}}(x,y) * g_k(x,y)|, \tag{6}$$

where f is a fractional factor, empirically set to 0.08, and $I_{\rm full}$ is the full, unpatch source image. Patches where $\bar{M}_{\hat{k}}$ does not exceed T are considered low confidence.

E. Wave Direction Calculation

The analysis yields the orientation of the wave crests, θ_{crest} . The direction of wave propagation, θ_{wave} , is orthogonal to the crest line. Therefore, the wave direction is determined by the equation $\theta_{wave} = \theta_{crest} + 90^{\circ}$.

IV. EXPERIMENT AND EVALUATION

The experimental process was designed in two stages. First, we validated the performance of the three proposed methods (standard, two-stage, and interpolation) on the synthetic grid benchmark images to determine their intrinsic accuracy under ideal, noise-free conditions. Second, the methods were applied to the real-world dataset from he coastal region along Chaloem Burapha Chonlathit road to evaluate their robustness and practical applicability.

For the quantitative evaluation on the synthetic benchmark, performance was assessed using several standard metrics, including mean absolute error (MAE), root mean square error (RMSE), and mean percentage error (MPE). Accuracy is specifically defined as the complement of the MPE, calculated as 100%-MPE. Additionally, to gauge the methods' ability to achieve high-precision results, we report the maximum error (the single worst-case deviation observed), the number of exact and near matches (error $\leq 0.1^{\circ}$), and the percentage of grid cells with a difference $\leq 0.5^{\circ}$.

For the real-world dataset, where conditions are more variable, evaluation focused on practical robustness. In addition to MAE and RMSE, we report the percentage of image patches with an estimated direction falling within $\pm 10^{\circ}$, within $\pm 20^{\circ}$, and within $\pm 30^{\circ}$ of the annotated ground truth. This set of metrics provides a practical measure of the algorithm's reliability for applications where a certain tolerance is acceptable.

A. Validation on Synthetic Benchmark

On the synthetic grid benchmark image, where the ground truth is perfectly known, the methods were evaluated using a comprehensive set of metrics. As shown in Table I, the two-stage method demonstrated exceptional performance, yielding the lowest MAE of 0.234° and the highest accuracy of 98.29%. It also correctly identified the exact orientation in two grids and had 14 near-perfect-match grids (i.e., the error $\leq 0.1^\circ$). This confirms that, under ideal conditions, the hierarchical search strategy is superior for achieving high-precision results. The interpolation method also performed well, while the standard method, as expected, had the highest error due to its limited angular resolution.

 $\label{thm:continuity} TABLE\ I$ Performance Metrics on the synthetic grid benchmark.

	Standard	Two-Stage	Interpolation
MAE (°)	1.453	0.234	0.432
RMSE (°)	1.676	0.283	0.756
MPE (%)	11.22	1.71	2.28
Accuracy (%)	88.78	98.29	97.72
Max Error (°)	2.980	0.600	2.970
No. of Exact Matches	0	2	1
No. of Near Matches ($\leq 0.1^{\circ}$)	2	14	16
Difference $\leq 0.5^{\circ}$ (%)	17.19	93.75	81.25

Examples of wave direction estimation using the two-stage refinement method are shown in Fig. 4.

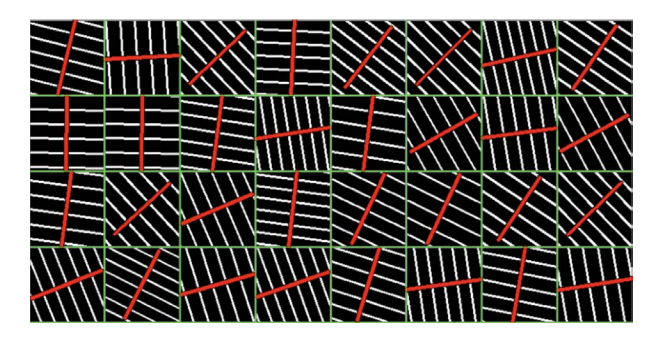


Fig. 4. Wave direction estimation results from the two-stage refinement method, illustrated on an 4×8 portion of the full 8×8 synthetic grid benchmark for clarity. Each red line represents the algorithm's high-precision output, demonstrating its performance under ideal, noise-free conditions.

B. Application to Real-World Imagery

When applied to the 403 patches of the Chaloem Burapha Chonlathit road dataset, the performance reflects the challenges of real-world conditions, including noise and variable wave patterns. The results are summarized in Table II. While the absolute error values are higher than on the synthetic data, the trend remains consistent, i.e., the refinement methods (two-stage and interpolation) outperform the standard approach. The interpolation method yielded the lowest overall error with an MAE of 12.95°, demonstrating it as a highly effective and efficient strategy for practical use. All methods successfully estimated the majority of wave directions to within $\pm 20^{\circ}$, confirming the general robustness of the Gabor filter framework.

To visually illustrate the performance on real-world data, Fig. 5 presents a collection of example patches organized by their estimation accuracy. In these examples, the yellow vector represents the ground truth direction established through manual annotation, while the red vector indicates the wave direction estimated by our algorithm. The figure showcases cases of high accuracy (angular error $\leq 10^{\circ}$), moderate accuracy (error $\leq 20^{\circ}$), and acceptable performance even in more complex scenes (error $\leq 30^{\circ}$). This visualization confirms the method's capability to identify the dominant wave orientation across a variety of real-world conditions.

TABLE II
PERFORMANCE METRICS ON
THE CHALOEM BURAPHA CHONLATHIT ROAD.

	Standard	Two-Stage	Interpolation
MAE (°)	13.23	12.96	12.95
RMSE (°)	15.63	15.24	15.22
Within ±10° (%)	37.72	39.21	38.96
Within $\pm 20^{\circ}$ (%)	79.65	81.39	81.14
Within $\pm 30^{\circ}$ (%)	96.77	97.27	97.27

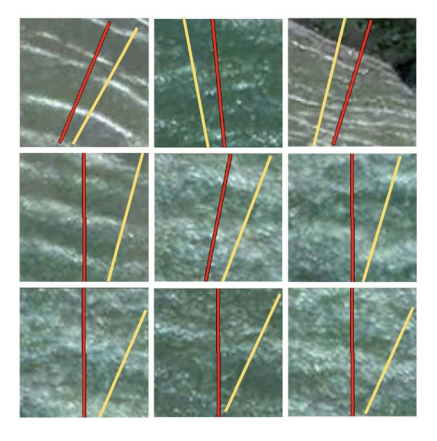


Fig. 5. Visual examples of wave direction estimation on real-world patches, categorized by angular error. Each row displays results within a specific error bound: (top) error $\leq 10^{\circ}$, (middle) error $\leq 20^{\circ}$, and (bottom) error $\leq 30^{\circ}$. The estimated wave direction is shown by the red vector, while the manually annotated ground truth is the yellow vector.

V. DISCUSSION

The practical implication of this work extends directly to coastal erosion management. The ability to automatically and repeatedly estimate nearshore wave direction from widely available satellite imagery provides a crucial, previously missing data layer. This information is vital for following purposes: (1) validating and calibrating hydrodynamic and sediment transport models, which often rely on offshore wave data that may not reflect local conditions; (2) explaining observed patterns of erosion and accretion, as wave direction is a primary driver of longshore sediment transport; and (3) informing the design and placement of coastal protection structures. Ultimately, this method offers a cost-effective tool for monitoring dynamic coastal processes, supporting more informed and adaptive management strategies.

Although the techniques performed well, several limitations merit discussion. First, the ground truth for the real-world dataset is based on manual annotation, which is inherently subjective. Future work could validate these results against in-situ measurements (e.g., from wave buoys) for a more objective assessment.

Second, the current method utilizes a fixed set of Gabor parameters. Furthermore, the precise spatial resolution (e.g., meters per pixel) of the imagery was not explicitly calibrated in this study. This combination presents a notable limitation, as optimal Gabor filter parameters particularly the wavelength (λ) are intrinsically linked to the physical scale of the wave

patterns. The lack of a defined scale makes it challenging to directly apply the empirically chosen pixel-based parameters to imagery from different sensors or altitudes, and future enhancements should explore adaptive parameter selection. n

Third, the analysis can be confounded by non-wave features such as sun glint or ship wakes. Integrating pre-processing steps like image segmentation could improve reliability [22]. A broader review of nearshore remote sensing techniques further contextualizes these challenges [12].

VI. CONCLUSION

This study proposed and rigorously validated a multi-stage Gabor filter analysis for wave direction estimation. By first testing on a synthetic benchmark, we confirmed the theoretical accuracy of the algorithms, identifying the two-stage method as the most precise under ideal conditions. Subsequent application to real-world coastal imagery from Thailand demonstrated the practical robustness of the framework, with the computationally efficient interpolation method proving to be a good choice for balancing accuracy and performance.

Our experiments show that while a standard Gabor analysis is effective, a refinement stage is crucial for enhancing accuracy. The proposed methods proved highly effective, with the two-stage refinement yielding a mean absolute error (MAE) of just 0.234° in ideal conditions, and the interpolation refinement achieving a robust 12.95° MAE on real-world data. The method is lightweight, interpretable, and suitable for operational wave monitoring. Future enhancements may include adaptive parameter selection for Gabor filters, integration of deep learning for improved water masking [22], and development of probabilistic models to handle ambiguous wave patterns more effectively [14], [23].

ACKNOWLEDGEMENT

The ASEAN IVO project (http://www.nict.go.jp/en/asean ivo/index.html), titled 'Coastal Erosion Monitoring Platform Based on Wireless Sensor Networks and 3D Point Clouds from Airborne LiDAR,' was involved in the production of the contents of this work and financially supported by NICT (http://www.nict.go.jp/en/index.html). This study is financially supported by Faculty of Informatics, Burapha University.

REFERENCES

- E. Bird, Coastal Geomorphology: An Introduction. John Wiley & Sons, 2008.
- [2] P. Suntra-rachun and A. Buranapratheprat, "Long-shore and rip currents during high tide at bangsaen beach, chonburi province," in *The 4th National Conference on Informatics, Agriculture, Management, and Environment*, 2017.
- [3] J. Phaksopa and P. Sojisuporn, "The analytical of wave characteristics and shoreline changes at tumbon kao roop chang, songkhla province in 2015 and 2016," Academia.edu, 2017.
- [4] N. Sannatai, S. Ritphring, and S. Prigboonchan, "Shoreline changes along phuket island," in 19 (The 19th Kasetsart University Kamphaeng Saen Campus National Conference). Nakhon Pathom, Thailand: Kasetsart University, Kamphaeng Saen Campus, dec 2022, pp. 481–493.
- [5] C. Chawalit, W. Boonpook, A. Sitthi, K. Torsri, D. Kamthonkiat, Y. Tan, A. Suwansaard, and A. Nardkulpat, "Geoinformatics and machine learning for shoreline change monitoring: A 35-year analysis of coastal erosion in the upper gulf of thailand," *Engineering and Applied Science Research*, vol. 52, no. 2, feb 2025.

- [6] P. Imlamai, S. Worachananant, and J. Phaksopa, "Monitoring study of coastal morphological change from coastal engineering structures at mrigadayavan palace, phetchaburi province using geo-informatics," *Burapha Science Journal*, vol. 28, no. 2, 2023.
- [7] A. Faiboon and W. Sangmanee, "Geospatial Monitoring and Forecasts of Coastal Engineering Structures' Shoreline Transformational Impact at Songkhla Lake Mouth," *Princess of Naradhiwas University Journal*, vol. 11, no. 3, pp. 165–179, 2019. [Online]. Available: https://li01.tci-thaijo.org/index.php/pnujr/article/view/160033
- [8] DHI, Coastal and Offshore Processes, Danish Hydraulic Institute, 2004.
- [9] P. D. Komar and D. L. Inman, "Longshore sand transport on beaches," *Journal of Geophysical Research*, vol. 75, no. 30, pp. 5914–5927, 1970.
- [10] L. Cavaleri, J.-H. Alves, F. Ardhuin, A. Babanin, M. Banner, K. Belibas-sakis, M. Benoit, M. Donelan, J. Groeneweg, T. Herbers *et al.*, "Wave modelling—the state of the art," *Progress in oceanography*, vol. 75, no. 4, pp. 603–674, 2007.
- [11] S. Vitousek, D. Buscombe, K. Vos, P. L. Barnard, A. C. Ritchie, and J. A. Warrick, "The future of coastal monitoring through satellite remote sensing," *Cambridge Prisms: Coastal Futures*, vol. 1, p. e10, 2023.
- [12] R. Holman and M. C. Haller, "Remote sensing of the nearshore," *Annual Review of Marine Science*, vol. 5, pp. 95–113, 2013.
- [13] W. Koch, "Directional analysis of sar images aiming at wind direction," IEEE Transactions on Geoscience and Remote Sensing, vol. 42, no. 4, pp. 702–710, 2004.
- [14] R. Almar, E. W. J. Bergsma, P. A. Catalán, M. J. Córcoles, D. Di Luccio, J. M. Fernández, M. González, A. N. Lerma, C. Martínez, R. Molina, and M. A. Romeu, "Sea state from single optical images: A methodology to derive wind-generated ocean waves from cameras, drones and satellites," *Remote Sensing*, vol. 13, no. 4, p. 679, 2021.
- [15] A. Pleskachevsky, C. Gebhardt, W. Rosenthal, and S. Lehner, "Multi-parametric sea state fields from synthetic aperture radar for maritime situational awareness," *Remote Sensing of Environment*, vol. 280, p. 113174, 2022.
- [16] F. Collard, F. Ardhuin, and B. Chapron, "Extraction of coastal ocean wave fields from sar images," *IEEE Journal of Oceanic Engineering*, vol. 30, no. 3, pp. 526–533, 2005.
- [17] A. Mahmoud, E.-S. Naser, and L. Henry, "Dual-modal approach for ship detection: Fusing synthetic aperture radar and optical satellite imagery," *Sensors* 2025, jan 2025.
- [18] D. A. Clausi, "Comparison and fusion of co-occurrence, gabor and mrf texture features for classification of sar sea-ice imagery," *Canadian Journal of Remote Sensing*, 2014.
- [19] C. Yushi, Z. Lin, G. Pedram, J. Xiuping, T. Liang, and L. Guoyu, "Hyperspectral images classification with gabor filtering and convolutional neural network," *IEEE Geoscience and Remote Sensing Letters*, 2017.
- [20] A. A. Yakimenko and A. I. Makfuzova, "Investigation of edge detection methods using the example of wave field pattern image," in *IOP Conference Series: Materials Science and Engineering*, vol. 1019, no. 1. IOP Publishing, 2021.
- [21] F. Bianconi and A. Fernández, "Evaluation of the effects of gabor filter parameters on texture classification," *Pattern Recognition*, vol. 40, no. 12, pp. 3325–3335, 2007.
- [22] M.-A. Blais and M. A. Akhloufi, "Advances in remote sensing and deep learning in coastal boundary extraction for erosion monitoring," *Geomatics*, vol. 5, no. 1, p. 9, 2025.
- [23] A. A. Fernandes, Y. V. B. Sarma, and H. B. Menon, "Wave directional spectrum from sar imagery," *Journal of the Indian Society of Remote Sensing*, vol. 28, pp. 175–190, 2000.